Petroleum Science 21 (2024) 2769–2778

Contents lists available at ScienceDirect

Petroleum Science

journal homepage: www.keaipublishing.com/en/journals/petroleum-science

Original Paper

Reliability analysis of carbon fiber rod-reinforced umbilical cable under tension using an improved sampling method

Yu Zhang [a, *], Hong-Yu Zhang [a], Ran Xia [b], Si-Ao Jiang [a], Fang Wang [c]

[a] College of Safety and Ocean Engineering, China University of Petroleum, Beijing, 102249, China
[b] China Academy of Aerospace Aerodynamics, China Aerospace Science and Technology Group, Beijing, 100094, China
[c] College of Engineering Science and Technology, Shanghai Ocean University, Shanghai, 201306, China

ARTICLE INFO

Article history:
Received 28 June 2023
Received in revised form
23 January 2024
Accepted 28 February 2024
Available online 1 March 2024

Edited by Jie Hao and Meng-Jiao Zhou

Keywords:
Umbilical cable
Carbon fiber rod
Failure analysis
Response surface method
Reliability

ABSTRACT

The umbilical cable is a vital component of subsea production systems that provide power, chemical agents, control signals et al., and its requirement for reliability is exceedingly high. However, as the umbilical cable is a composite structure comprising multiple functional units, the reliability analysis of such cables involves numerous parameters that can impact calculation efficiency. In this paper, the reliability analysis of a new kind of umbilical cable with carbon fiber rod under tension is analyzed. The global dynamic analytical model is first established to determine the maximum tension load, then the local analytical model of umbilical cable including each unit are constructed by finite element method (FEM). Based on the mechanical analytical model, the reliability of umbilical cable under tension load is studied using response surface method (RSM) and Monte Carlo method. During the calculation process, a new tangent plane sampling method to calculate the response surface function (RSF) is proposed in this paper, which could make sampling points faster come close to the RSF curve, and it is proved that the calculation efficiency increases about 33% comparing with traditional method.

1. Introduction

The umbilical cable is a crucial component of underwater control and umbilical cable systems. It is a composite cable consisting of hydraulic pipes, cables, optical fibers, chemical conduit, etc. Its primary function is to establish a connection between the main production platform and underwater system equipment, providing electrical, hydraulic power, control data signals, and chemical injection channels for subsea manifold systems and oil wellheads. It serves as the “nerve center” for oil and gas extraction (Guo, 2016). The umbilical cable is subjected to complicated loads during operation, including gravity, waves, currents, platform motion, and others. As a result, tension failure, fatigue failure, buckling and sail failure may occur in the umbilical cable (Thies et al., 2012). Therefore, it is necessary to study the mechanical properties and reliability of the umbilical cable.

Many scholars have conducted research on the mechanical properties of the umbilical cable. Knapp derived the equilibrium equation of geometric nonlinearity, the linear stiffness matrix, the stress equation of armored steel wire inside the umbilical (Knapp, 1975, 1979, 1981). Sævik and Gjøsteen (2012) proposed a three-dimensional finite element formulation to predict the performance of complex umbilical sections under tension, torque, internal pressure and external pressure. Lu (2013) developed predictive models for the tensile, bending, and fatigue behavior of umbilical cables using the Abaqus pseudo-static analytical method. Zhu (2017) developed a three-dimensional solid finite element method (FEM) of an umbilical cable, simulated various combined loading conditions, and analyzed the effects of different loads on the cable's mechanical properties. Tang et al. (2014) and Zhao (2017) analyzed the tensile behavior of umbilical cables using finite element analysis and calculated the probability of cable failure under in-situ conditions. Liu et al. (2018) explored the influence of the internal filler and tensile rate of the umbilical cable on its tensile properties. The results show that the filling unit and the tensile rate have a certain influence on the tensile stiffness of the umbilical cable, but the influence on the mechanical properties of the umbilical cable section is small. Zhang et al. (2019) used FEM software to analyze the sensitivity of parameters affecting the static

* Corresponding author.
E-mail address: zhangyu@cup.edu.cn (Y. Zhang).

https://doi.org/10.1016/j.petsci.2024.02.016

Nomenclature

Symbol	Definition
Z_1	The tensile failure function of the umbilical cable
S_y	Yield strength
p	The maximum stress of steel tube unit
$\widehat{g}(X)$	The quadratic polynomial function without cross terms
a, b, c	Constants
β	Reliability index
x	Random variables
X	The vector of random variables
μ_i	The mean of random variables
σ_i	The standard deviation of random variables
$g(X)$	RSF
X_μ	The mean vector of random variables
X_D	Check points
η	The unit vector of $w = X_D - X_\mu$
X_i^C	Intersection points
$X_i^{(0)}$	Indirect points
ξ_i	The unit vector of the reconstructed vector

strength of umbilical cables, while considering the effect of friction. Wang et al. (2021) developed a three-dimensional nonlinear finite element model for deep-sea non-metallic armored umbilical cables based on precise geometric beam theory and the principle of virtual work. Yang et al. (2023) investigated the mechanical properties, particularly the top tension, of deep-sea umbilical cables during deployment and retrieval. Their research was based on the integration of three-dimensional potential flow theory and the concentrated mass method, accounting for the combined influences of surface-supported vessel motion and ocean currents.

Due to the complex structure, laborious manufacturing process, and numerous functional units of an umbilical cable, there is randomness in the geometric and material parameters that can affect the cable's reliability. Nilsen and Hanson (1995) established a correlation between the failure probability, derived from the deterministic safety factor design method, and the uncertainty associated with random variables. As an illustrative case, they examined a 15-inch flexible riser located at a depth of 330 m underwater. By considering the uncertainty distribution of environmental load variables and riser structural parameters, they confirmed the existence of discrepancies between the safety factor and the corresponding failure probability. Akpan et al. (2007) and Xia and Das (2008) proposed a fatigue reliability calculation method that considers the uncertainties of material parameters, damage index, and structural load, and used the first-order second moment method to calculate the fatigue reliability. Song et al. (2011) focused on the reliability-based design optimization (RBDO) of the riser support system for a floating production storage and offloading unit (FPSO) during operation, extreme conditions, and in the presence of damage or pipeline failures. Within the RBDO framework, they employed RSM and applied the moving least squares method to obtain the optimal probabilistic solution. Yan et al. (2018) analyzed the strength reliability of the critical section of an umbilical cable using an improved first-order second moment method and Monte Carlo method. Xia et al. (2021) used the fuzzy fault tree method to calculate the reliability of an umbilical cable and concluded that the sheath/armor has the greatest impact on the cable's reliability. Zhang et al. (2021a) analyzed the probability of torsional instability of flexible pipeline by both the first-order second moment method and Monte Carlo method. Xu (2019) employed the equivalent normalization method and Monte Carlo simulation to calculate the reliability of an umbilical cable. Zhang et al. (2021b) employed a multi-stage Bayesian network to predict the reliability of an umbilical cable.

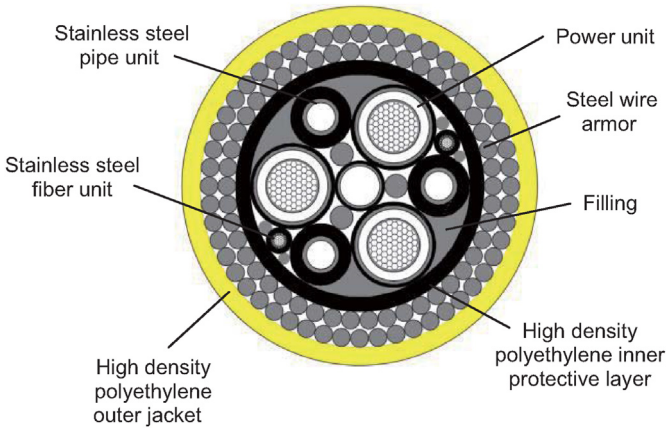

Fig. 1. Typical umbilical cable.

The steel tension armor of the umbilical cables in the above research consists of two layers with opposite helical angles, as shown in Fig. 1. However, as the water depth increases, the weight of the steel tension armor also increases, which may lead to the tensile failure of the umbilical cable. The carbon fiber rod reinforced umbilical cable, shown in Fig. 2, replaces the steel tension armor with carbon fiber rods. This modification significantly reduces the weight of the cable and improves its tensile and bending resistance (Yu and Su, 2008). In order to effectively utilize the new type of umbilical cable, it is essential to analyze its mechanical properties and reliability.

2. The mechanical analysis of carbon fiber rod reinforced umbilical cable

The model of the carbon fiber rod reinforced umbilical cable shown in Fig. 2 was constructed using Abaqus software. The geometric parameters and quantities of each unit in the umbilical cable are shown in Table 1, and the material properties of each unit are shown in Table 2.

In the FEM model of umbilical cable, the electric cable was simplified as a copper core wrapped with high density polyethylene, and the optical fiber unit was simplified as a steel shell wrapped with high-density polyethylene. The simplified model of

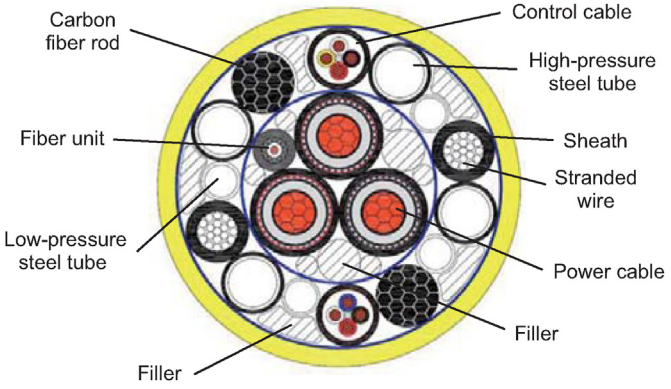

Fig. 2. Carbon fiber rod reinforced umbilical cable.

Table 1
Geometry parameters of umbilical cable.

Name	External diameter, mm	Wall thickness, mm	Number
High pressure hydraulic pipe	12.7	1.3	4
Low pressure hydraulic pipe	19.05	1.3	4
Stranded wire	19	x	2
Carbon fiber rod	24.4	x	2
Power cable	185 mm^2 (Conductor section)	x	1
Control cable	24.4 (Outside diameter)	x	2
Optical fiber	Single mode, 16 channels	x	1

Table 2
Material parameters of umbilical cable.

Function unit	Material	Elastic modulus, MPa	Poisson's ratio
Steel tube	Super duplex stainless steel	206,000	0.33
Stranded wire	Steel	195,000	0.33
Filling and each unit sheath	High density polyethylene	1200	0.48
Electric cable	Copper	110,800	0.33
Carbon fiber rod	T700 carbon fiber	210,000 (Equivalent parameter)	0.307 (Equivalent parameter)

umbilical is shown in Fig. 3.

The contacts between the units in the model were defined as general contacts, which were considered as hard contacts. One end of the model was fixed while the other end was subjected to loads, and a reference point was established at the end to constrain the end section at the reference point. The model utilized hexahedral elements with C3D8R grid type. The meshes for steel tubes, stranded wires, and carbon fiber rods were refined to accurately capture their load-bearing characteristics. Fig. 4 shows the meshed umbilical cable.

The FEM model described above was used to apply tension, bending moment, and torsion loads to the end of the umbilical cable, and obtain its stiffness properties. The resulting tension stiffness (K_T), torsional stiffness (K_B), and bending stiffness (K_N) were 385 MN, 21.9 kN m^2, and 15.3 kN m^2, respectively.

For the study of theoretical stiffness models for helically wound structures, Knapp (1981) provided a theoretical formula (Eq. (1)) for the tensile strength of helical structures, and he presented the expression (Eq. (2)) for torsional stiffness excluded radial deformation for helically wound structures.

$$K_T = (AE)_0 + \sum_{i=1}^{n} (AE)_i \left(1 - \frac{R_c}{2R_i} \mathrm{tg}^2 \alpha_i\right) \cos^3 \alpha_i \tag{1}$$

$$K_N = (IG)_0 + \sum_{i=1}^{n} E_i A_i R_i^2 \sin \alpha_i^2 \cos \alpha_i \tag{2}$$

where, $(AE)_0$ represents the tensile stiffness of the central conductor, A represents the cross-sectional area of the structure, E represents the elastic modulus, $(AE)_i$ represents the tensile stiffness of the ith helical structure, R_i represents the distance from the helical structure to the center of the cylinder, R_c represents the radius of the core, α_i is the winding angle of the helical structure, $(IG)_0$ represents the torsional stiffness of the central conductor, I represents the moment of inertia, G represents shear modulus, and R_i denotes the radius of each structure.

Costello (1997) examined a single helical structure extracted from the overall umbilical cable model. By ignoring interactions between elements, he determined the bending stiffness of a single free helical structure under pure bending. Summing contributions from all elements, Costello derived the overall bending stiffness formula (Eq. (3)) for the entire structure.

$$K_B = (EI)_0 + \sum_{i=1}^{n} \frac{2E_i I_i \cos \alpha_i}{2 + \upsilon_i \sin \alpha_i^2} \tag{3}$$

where υ_i denotes the Poisson's ratio of the helical structure.

Upon substituting the relevant material and dimensional data for each component of the carbon fiber rod-reinforced umbilical cable in Fig. 1(b), theoretical values for tensile stiffness, bending

Fig. 3. The FEM model of carbon fiber rod reinforced umbilical cable.

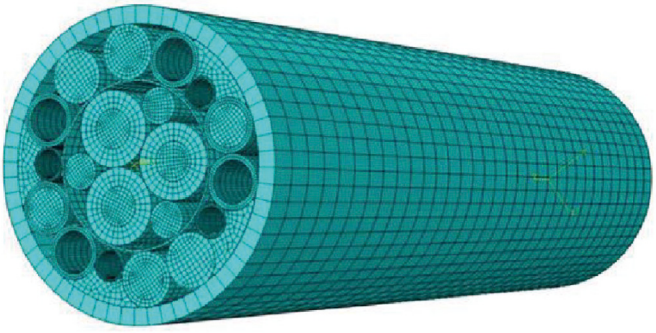

Fig. 4. The meshed model of carbon fiber rod reinforced umbilical cable.

stiffness, and torsional stiffness were obtained. A comparison between these theoretical values and the finite element model calculation results are presented in Table 3.

There is a relative error between theoretical calculations and finite element results, and this discrepancy is attributed to assumptions in the stiffness theoretical model, including the neglect of interactions among internal components. The comparison of tension stiffness, torsional stiffness and bending stiffness between theoretical and finite element results verified the validity of the mechanical model.

To analyze the mechanical properties of umbilical cable under tension loads, the global analysis was conducted to determine the maximum tension load that the cable could withstand. The global model was constructed using OrcaFlex software. The umbilical cable analyzed in this study is designed for use at a water depth of 2000 m and employs a lazy wave configuration (Fig. 5) to effectively mitigate top tension (Chen et al., 2018). The length of umbilical cable from top spar platform to the buoyant cylinder AB = 2300 m, the buoyant length BC = 150 m, and the length from buoyant cylinder to seabed CD = 150 m. The horizontal distance from the suspension point to the touch point E = 600 m, and the depth H = 2000 m. The friction coefficient between umbilical cable and seabed and the seabed stiffness are shown in Table 4.

The description of waves typically involves two types: regular waves and irregular waves. Regular waves are primarily derived from fluid mechanics theory and are characterized by parameters such as wave direction, wave height, period, and starting time. The most commonly used regular wave theories include linear wave theory (Airy wave), Stokes wave theory, Dean wave theory, and elliptic cosine wave theory. On the other hand, irregular waves are typically described based on statistical random spectra. Various methods for superimposing regular waves are often employed to represent irregular waves, such as the PM spectrum and JONSWAP spectrum (Guo, 2016).

When selecting wave types for model analysis, the analysis type and actual sea conditions are the main factors considered. In order to simplify the calculation process, this paper utilizes a regular wave in the model to analyze and calculate the dynamic response of the umbilical cable. The aforementioned regular wave theories are applicable to different water depths. In this model, the seawater depth is 2000 m, which is suitable for the use of linear wave theory (Airy wave).

For specific wave loads and to ensure a more conservative calculation of reliability, the chosen sea state parameters are based on a 100-year return period. The selected location is a specific operating zone in the South China Sea. In this zone, the maximum impact of the ocean currents is observed to flow from east to west by Zhao et al. (2022). Therefore, the current direction was selected as 270° in OrcaFlex software. The corresponding values are presented in Table 5.

The velocity of seawater is typically influenced by both the velocity of the ocean surface and the depth of the water. In cases where specific current data is not available, the current velocity $V_C(Z)$ at a given water depth z can be estimated using the profile calculation method 1, as proposed by Xing et al. (2012). This method allows for the estimation of current velocities based on certain assumptions and calculations.

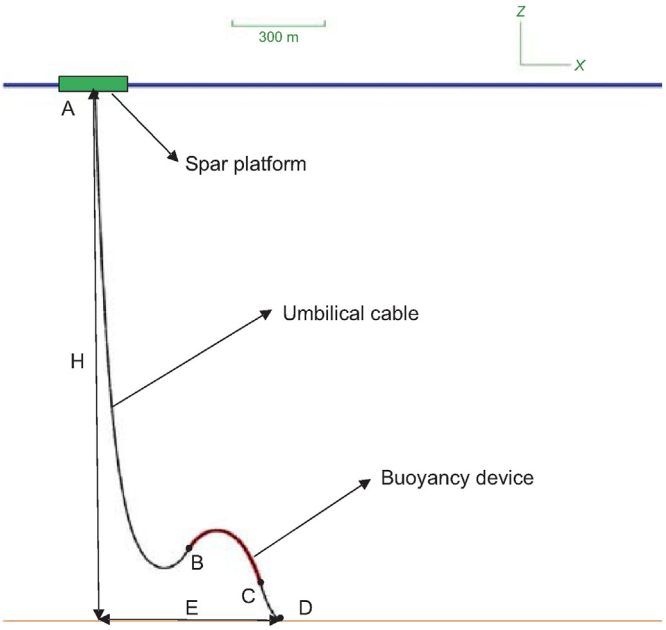

Fig. 5. The global model of carbon fiber rod reinforced umbilical cable.

Table 4
The friction coefficient and seabed stiffness.

Coefficient	Values
Normal friction coefficient	0.9
Axial friction coefficient	0.35
lateral rigidity, kN/m	100
Shearing rigidity, kN/m	100

$$V_C(Z) = V_C(0)\left[\frac{H-z}{H}\right]^{\frac{1}{7}} \tag{4}$$

By utilizing the aforementioned formula, the seawater velocity at various depths can be calculated for the current load with a 100-year return period. The specific parameters related to the current are listed in Table 6.

The tension loads along the axial length of umbilical cable are shown in Fig. 6 including the maximum, minimum and mean values. The findings indicate a decrease in the tension load of the umbilical cable along its axial length, with an increase at the buoyancy section. The highest tension load is observed at the top of the umbilical cable, with a value of 138 kN.

After applying a tension load of 138 kN to the finite element model (Fig. 3) that has been validated in the above, the stress distribution of the umbilical cable was analyzed and is presented in Fig. 7. The results indicate that the highest stress is observed in the carbon fiber rod, followed by the stranded wire and steel tube. The stresses in the sheath and fillings are negligible, as expected.

Table 3
Comparison between theoretical and finite element results.

Stiffness	Theoretical results	Finite element results	Relative error
Tensile stiffness	404.1 MN	385 MN	4.7%
Bending stiffness	22.3 kN m^2	21.9 kN m^2	1.8%
Torsional stiffness	17.4 kN m^2	15.3 kN m^2	12.6%

Table 5
Ocean environment parameters (Once per 100 years).

Parameters	Values
Maximum wave height, m	13.4
Period of maximum wave height, s	14.7
Surface flow velocity, m/s	2.04
Underflow velocity, m/s	0.3

Table 6
The friction coefficient and seabed stiffness.

Surface velocity, m/s	2.04	
Current direction, deg	270	
Flow velocity	Water depth, m	Value, m/s
	0	2.040
	100	2.025
	350	1.985
	500	1.958
	1000	1.848
	1300	1.756
	1750	1.516
	1900	1.330
	2000	0

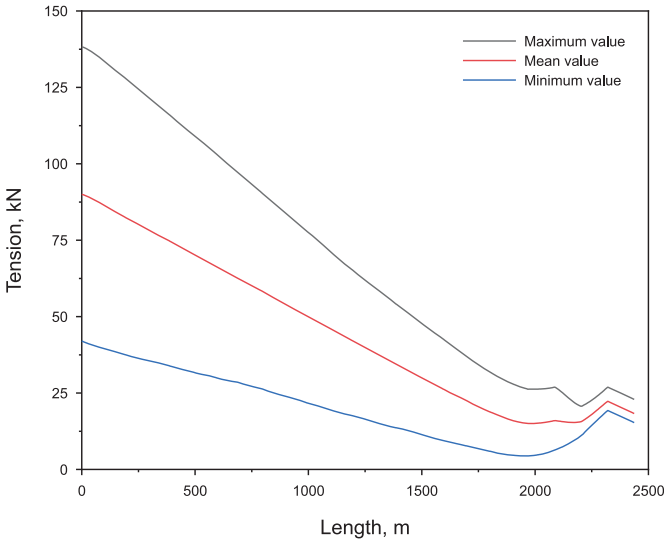

Fig. 6. The tension load along the axial length of umbilical cable.

In finite element analysis, the size and quantity of the mesh have a significant impact on the accuracy of the computational results. Therefore, a mesh-independence validation, as illustrated in Fig. 8, was conducted for the established model. It can be observed that the maximum stress almost stabilizes when the number of grids approaches around 240,000. The maximum stress obtained is listed in Table 7.

The stress utilization ratio N in this paper is the product of the safety factor n ($n = 1.5$) and the maximum stress divided by the yield stress, indicates the failure priority. If $N = 1$, the maximum stress equals to the yield stress, which means the failure will happen. Table 7 shows the stress utilization ratio N for each unit of the umbilical cable. It can be seen that the ratio of stress utilization of the steel tube is much larger than other units, so its failure priority is 1, which means that tensile failure may firstly happen in the steel tube unit.

Therefore, the following reliability analysis of umbilical cable in this paper is based on the steel tube mechanical analysis.

3. Reliability analysis of umbilical cable under tension loads

The tensile failure function of umbilical cable is defined as

$$Z_1 = S_y - np \tag{5}$$

where, S_y represents the yield strength, p represents the maximum stress. As discussed in the above, the first priority of tension failure is steel tube, the parameters of S_y and p are the parameter values of steel tube, and n represents the safety factor, taking 1.5 in this paper. When $Z_1 > 0$, it means the umbilical is safe, and tension failure will not happen. The reliability calculation is to calculate the probability of $P\{Z_1 > 0\}$.

From Tables 7 and it is seen that the maximum value is smaller than the yield stress, which looks like the reliability is 100%. However, the geometry parameters and material parameters of umbilical cable have some randomness during manufacture and process, which can induce the randomness of S_y and p. So, the randomness has to be considered during the reliability analysis. In this paper, the thickness of steel tube, diameter of stranded wire, diameter of carbon fiber rod and tensile strength of steel tube are considered as random variables, assumed to follow a normal distribution. The statistical characteristics of each variable are shown

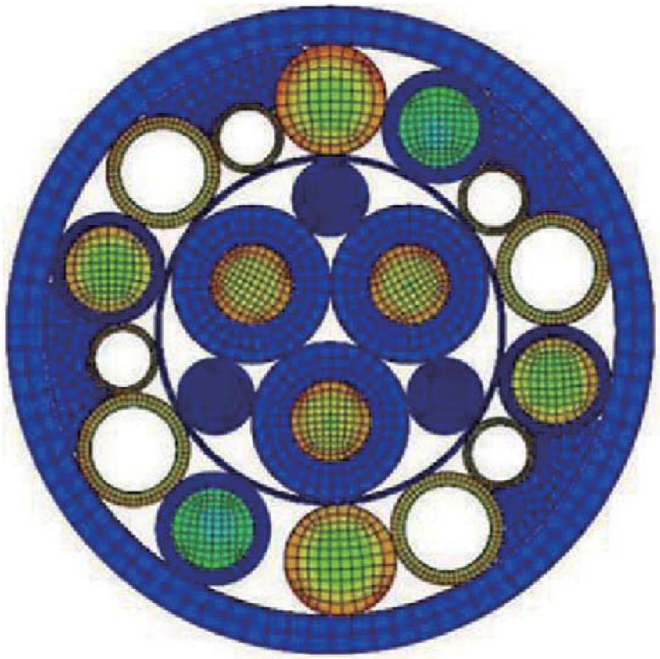

Fig. 7. Stress nephogram of umbilical cable.

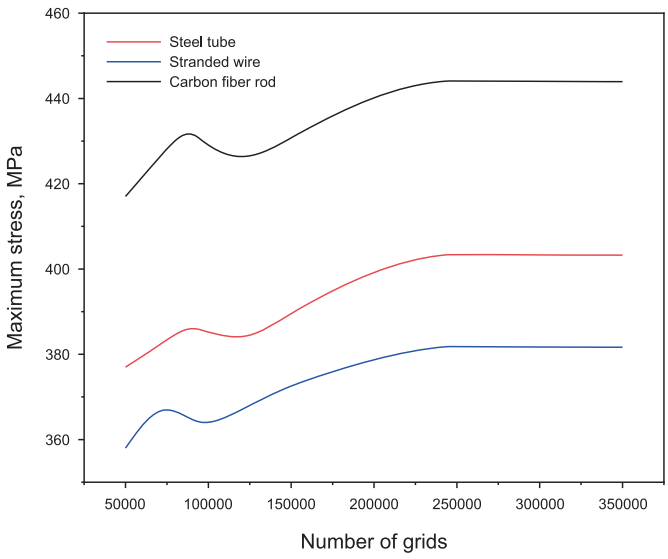

Fig. 8. The variation of maximum stress with the number of grids.

Table 7
The maximum stresses and failure priority of different units.

Unit	The maximum stress, MPa	Yield stress, MPa	N	Failure priority
Steel tube	403.4	670	0.903	1
Stranded wire	381.9	1270	0.451	2
Carbon fiber rod	444.2	2700	0.247	3

in Table 8.

3.1. Classical RSM

To calculate the probability of $P\{Z_1 > 0\}$, it is necessary to know the relationship between the tensile strength of steel and the thickness of steel tube, diameter of stranded wire, diameter of carbon fiber rod, and tensile strength, which cannot be obtained directly. In practical engineering, the RSM is often used to obtain an approximate function instead of the real function (Liu and An, 2020). In the RSM, a shape of the function with several undetermined parameters is first assumed, and then the relationship between the undetermined parameters and the random variables is obtained through FEM simulation. During the calculation process, sample points of the random variables are given, and iterative calculation is performed until the error is satisfied. The process of using the classical RSM to fit the structural performance function is as follows:

(1) The selection of RSF type

The quadratic polynomial function without cross terms (shown in Eq. (6)) was selected as the type of RSF, which has higher fitting accuracy and fewer undetermined coefficients.

$$\hat{g}(x) = a_0 + \sum_{i=1}^{m} b_i X_m + \sum_{i=1}^{n} c_i X_n^2 \tag{6}$$

where, a_0, b_i, c_i is the undetermined coefficient in the RSF.

(2) Select sample points to fit the RSF

Once the form of the RSF has been determined, the selection and fitting process of sample points can be carried out using the following steps:

The initial iteration center point is denoted as $X^{(1)} = (x_1^{(1)}, x_2^{(1)}, \ldots, x_n^{(1)})$. To calculate the output value Z, the mean point of each variable is taken, resulting in $Z = g(x_1^{(1)}, x_2^{(1)}, \ldots, x_n^{(1)})$. Additionally, by varying each variable around its mean point, $Z = g(x_1^{(1)}, x_2^{(1)}, \ldots, x_i^{(1)} \pm f\sigma_i, \ldots, x_n^{(1)})$, where σ_i represents the standard deviation of each random variable. This process yields a total of $2n+1$ output variables.

The coefficient f typically varies throughout the iterative process. In the first generation, its value is set to 1, and then it is increased to 3 in subsequent generations.

Based on the provided sample points and outputs, the least squares method can be employed to solve the $2n+1$ undetermined coefficients in Eq. (6). The fitted response surface function can be calculated using either the moment method or the Monte Carlo method. This enables the determination of the checking point $X^{*(k)}$ and the reliability index β^k, where k represents the k th iteration. The convergence condition is assessed as follows:

$$\varepsilon = \left|\beta^{k+1} - \beta^k\right| \leq 0.01 \tag{7}$$

If the aforementioned convergence condition is satisfied, then β^{k+1} represents the final reliability index. If the condition is not met, the next generation iterative center point $X^{(k)}$ and other sample points are determined in the vicinity of the checking point $X^{*(k)}$. Eventually, when the convergence condition is satisfied, the calculation comes to a halt.

3.2. The improved RSM based on tangent plane sampling

However, as the shape of RSF is unknown, it is determined through initial sample points and many interaction times to come close the shape of RSF, but the calculation has poor fitting efficiency, and even non-convergence. The fitting process is shown in Fig. 9.

Therefore, we propose a new method to quickly come close to the shape of RSF based on the tangent plane. Firstly, the checking point X_D and tangent plane are determined by sequence interpolation along specific direction. Then, the indirect point $X_i^{(0)}$ of the sample points are selected based on the tangent plane, and the sample points are calculated by the indirect points. Compared with the conventional method, the sample points obtained in this way are close to the RSF faster, which can make the fitting process more efficient. The calculation process is depicted in Fig. 10, while the fitting process is presented in Fig. 11.

(1) The selection of RSF type

The quadratic polynomial without cross-terms simplifies the computational model, effectively addressing convergence issues. Additionally, the parameters mentioned earlier are mutually independent. Therefore, the response function model of the improved RSM utilizes a quadratic polynomial response without cross terms. The calculated adjusted coefficient of determination is $R^2 = 0.8541$, which further substantiates the strong fitting performance of the chosen model.

(2)The selection of initial sample points and the calculation of reliability index β_1.

With the mean point as the center, the test points were

Table 8
Parameters of random variables.

Random variable	Distribution	Mean value	Coefficient of variation	Standard deviation
Thickness of steel tube t	Normal distribution	1.3 mm	0.03	0.039
Diameter of stranded wire d_1	Normal distribution	19.0 mm	0.03	0.570
Diameter of carbon fiber rod d_2	Normal distribution	24.4 mm	0.03	0.732
Tensile strength of steel tube p	Normal distribution	670 MPa	0.03	18.67

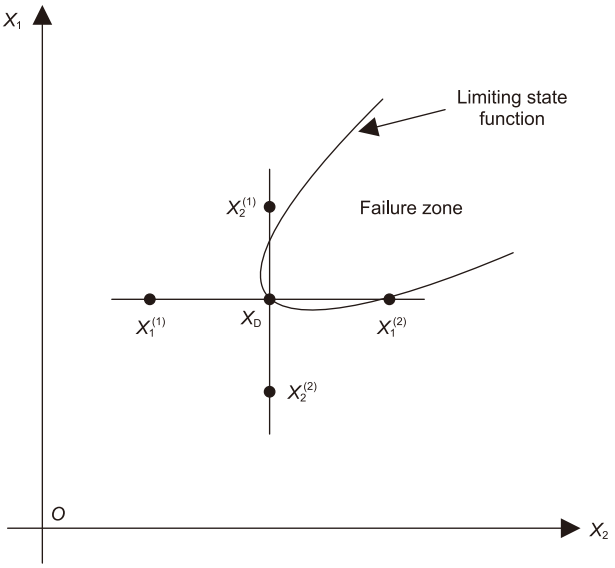

Fig. 9. Classical RSM fitting process.

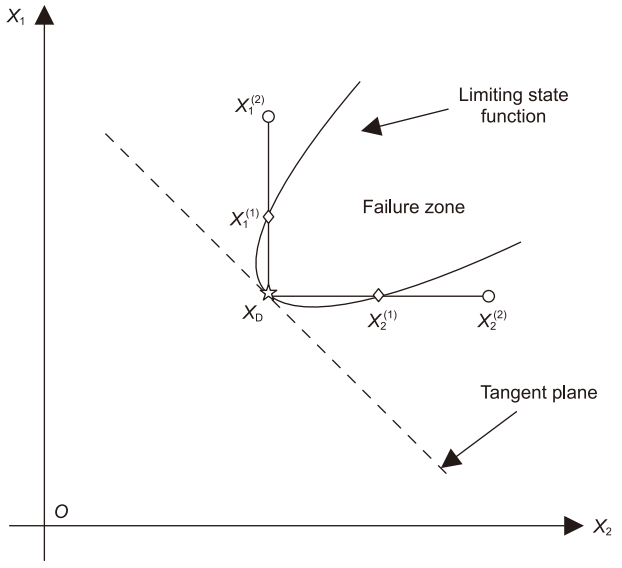

Fig. 11. Improved RSM fitting process.

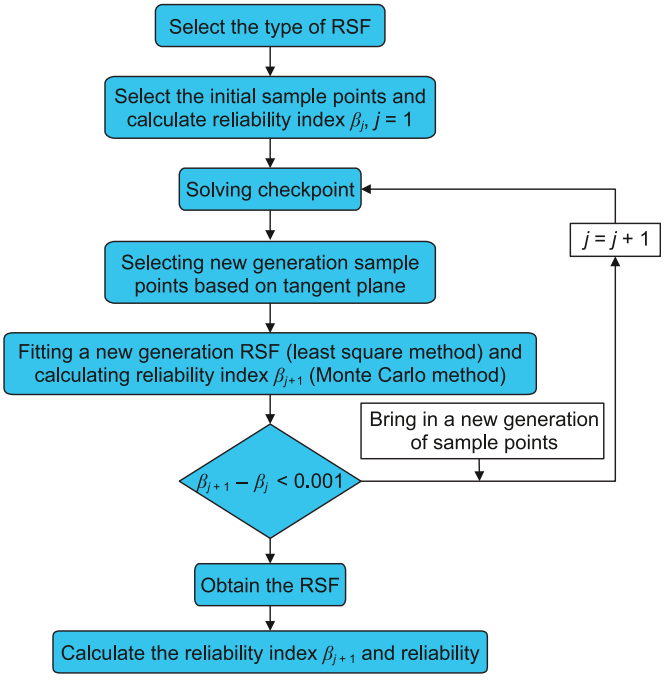

Fig. 10. The reliability calculation process with the improved RSM.

arranged along the positive and negative directions of each coordinate axis, and a total of $2n + 1$ test points were obtained:

$$X_1 = X_\mu = (\mu_1, \mu_2, \ldots, \mu_n)^{\mathrm{T}} \tag{8}$$

$$X_i = (\mu_1, \mu_2, \ldots, \mu_i - 3\sigma_i, \ldots, \mu_n)^{\mathrm{T}}, i = 1, 2, 3, \ldots, n; j = i + 1 \tag{9}$$

$$X_j = (\mu_1, \mu_2, \ldots, \mu_i + 3\sigma_i, \ldots, \mu_n)^{\mathrm{T}}, i = 1, 2, 3, \ldots, n; j = i + n + 1 \tag{10}$$

where, X_μ is the mean vector of random variables; μ_i and σ_i are the mean and standard deviation of random variable x_i; n is the number of random variables. β is the reliability index, it is defined as the following Eq. (11):

$$\boldsymbol{\beta} = \varphi^{-1}\left(p_{\mathrm{f}}\right) \tag{11}$$

where, p_{f} is the failure probability of umbilical cable.

The response values of $2n + 1$ sample points and each sample point were used to fit the first-generation RSF $g(X)$ by least square method, and the reliability index of the first-generation RSF β_1 was obtained by Monte Carlo method.

(3) The solution of checkpoint

Using the first-order second moment method to calculate the mean value and standard deviation of the first-generation RSF, the initial check point was obtained, denoted as X_{DL}. The following iterative method was used to select the checkpoint, ensuring a specific range between the checkpoint and the RSF:

$$X_{i+1} = X_i + \frac{X_{i-1} - X_i}{g(X_i) - g(X_{i-1})} g(X_i) \tag{12}$$

where, $g(X_i)$ is the function value of the RSF at point X_i. When $i = 1$, X_0 is X_μ, X_1 is X_{DL}. The convergence condition of this sequence interpolation is

$$\left|\frac{g(X_i)}{g(X_\mu)}\right| \leq \varepsilon \tag{13}$$

where, ε is the accuracy of checking point selection, which takes 0.001 in this paper.

The sample points satisfying the convergence condition was recorded as X_{D}, which is the checking points of the final selected RSF.

(4) The selection of new generation sample points

Firstly, constructed a vector $w = X_{\mathrm{D}} - X_\mu$, and its unit vector was denoted as η, which is the normal vector of the tangent plane of the RSF curve at the checking point. Then the tangent plane could be

obtained:

$$\eta^{\mathrm{T}}(X - X_{\mathrm{D}}) = 0 \tag{14}$$

The tangent plane of response surface at the checking point intersects with the coordinate axes of each random variable, and the intersection point was recorded as X_i^{C}, $i = 1, 2, \cdots$. The unit vector of the reconstructed vector was denoted as ξ_i, and the indirect point $X_i^{(0)}$ was arranged along the direction of the vector ξ_{i} based on the check point X_{D}. Since the area near the checkpoint has a great influence on the accuracy of the fitted RSF, the sample points were selected with the coefficient $0.5\sigma_i$, that is, the sample points from the checkpoint $0.5\sigma_i$ were selected on the tangent plane:

$$X_i^{(0)} = X_{\mathrm{D}} + 0.5\sigma_i \cdot \xi_i \ldots i = 1, 2, \ldots, n \tag{15}$$

where, σ_i is the standard deviation of the ith random variable.

Compare the symbols $g(X_i)$ and $g(X_\mu)$. If the two symbols have the same sign, the sample points $X_i^{(1)}$ are selected along the η direction based on X_i according to Eq. (16):

$$X_i^{(1)} = X_i^{(0)} + 0.5\sigma_i \cdot \eta \ldots i = 1, 2, \ldots, n \tag{16}$$

If the two symbols are opposite, the sample points $X_i^{(1)}$ are selected based on X_i in the opposite direction of η according to Eq. (17):

$$X_i^{(1)} = X_i^{(0)} - 0.5\sigma_i \cdot \eta \ldots i = 1, 2, \ldots, n \tag{17}$$

In addition, the last $2n$ sample points were selected with $X_i^{(1)}$ as the checking point and $X_i^{(2)}$ as the midpoint, which can make the final two points faster close to the response surface when the value of the random variable changes greatly, and can greatly increase the fitting efficiency.

$$X_i^{(2)} = X_i^{(1)} + \frac{X_i^{(1)} - X_{\mathrm{D}}}{2} = \frac{3X_i^{(1)} - X_{\mathrm{D}}}{2} \tag{18}$$

Finally, a total of $2n + 1$ sample points of X_{D}, $X_i^{(1)}$ and $X_i^{(2)}$ were obtained.

(5) The determination of RSF and the calculation of reliability

Using the final sample points, the RSF were determined, and the reliability and reliability index were calculated using Monte Carlo method.

The method proposed in this paper, which selects sample points based on the tangent plane, has been shown to improve the efficiency of sample point selection, reduce the number of required iterations, and enhance the fitting efficiency.

3.3. The reliability of umbilical cable

Using the improved RSM introduced in the above, the mean value of each random variable was used as the first-generation fitting center point to construct the sample point, and 7 sample points were obtained (Table 9). Subsequently, the FEMs of the umbilical cable for these 7 sample points are established individually, and the maximum stresses of the steel tube unit with each sample point were obtained in Table 9.

Based on the above seven sample points and their response values, through the improved RSM shown in Fig. 8, the final RSF Z_1 were obtained as shown in Eq. (19).

$$Z_1 = \frac{p}{1.5} - (-848.949 + 121.940t - 23.926d_1 + 140.311d_2) - 55.556t^2 + 0.410d_1^2 - 3.240d_2^2 \tag{19}$$

where, p is the maximum stress of steel tube unit, t is the thickness of steel tube, d_1 is the diameter of stranded wire, and d_2 is the diameter of carbon fibre rod.

Finally, the reliability and reliability index of umbilical cable under tension load were calculated, as shown in Table 10. It can be seen that the reliability of the carbon fibre reinforced umbilical cable under tension load is 0.99331, and the reliability index is 2.478. Based on the lack of reliability design guidelines for marine flexible pipelines, this paper makes reference to GB-50153-2008 (2008) and observes that the reliability index of flexible pipelines under the aforementioned conditions is significantly lower than the value of 4.2 specified therein.

Table 11 shows the comparison of results and calculation efficiency between the improved method and conventional method. The reliability index changing with iteration times are shown in Fig. 12. It can be found that the improved method is convergent after 6 iteration times, while it is 9 times for the conventional methods. Each iteration requires 7 sample points, that is, 7 finite element models need to be established in each iteration calculation. Therefore, 21 FEM models are reduced using the improved method, with the calculation efficiency increasing 33%.

In this study, the reliability of the umbilical cable is evaluated through the combination of mechanical analysis, RSM, and Monte Carlo method. The proposed new method for selecting sample points based on the tangent plane in the RSM is shown to be efficient and effective in reducing the number of FEM models required for constructing the RSF and increasing the calculation efficiency. This method could be applicable to other reliability calculation problems, particularly those with a large number of random variables, which may further increase the calculation efficiency. Future work could investigate the generalizability of this method to different types of engineering problems and explore the potential for further efficiency improvements through optimization.

4. Conclusions

In this paper, the mechanical properties and reliability of carbon fiber rod reinforced umbilical cable are analyzed, and the following conclusions are obtained.

(1) The global and local analytical models of the carbon fiber reinforced umbilical cable have been constructed. The maximum tensile load of the cable has been calculated to be 138 kN, and the stress utilization ratio (N) of different units in the umbilical cable are compared. The steel tube has the largest ratio 0.903, indicating that the steel tube is the first unit to fail.
(2) The RSF of the umbilical cable under tension load is obtained considering the randomness of thickness of steel tube, diameter of stranded wire, diameter of carbon fiber rod and tensile strength of steel tube. During the interaction calculation process, the selecting sample point method is improved, which can make the sample points faster close to the response surface curve.
(3) The reliability of umbilical cable calculated by the improved RSM is 0.99331 and the reliability index is 2.478. The interaction times is 6 with 42 sample points, while it is 9 with 63 sample points for the conventional method. It is proved that

Table 9
Sample points and response values.

Sample point	Thickness of steel tube t, mm	Diameter of stranded wire d_1, mm	Diameter of carbon fiber rod d_2, mm	The maximum stress of steel tube unit p, MPa
1	1.300	19.000	24.400	400.3
2	1.417	19.000	24.400	385.1
3	1.183	19.000	24.400	406.5
4	1.300	20.710	24.400	397.8
5	1.300	17.290	24.400	411.3
6	1.300	19.000	26.596	404.9
7	1.300	19.000	22.204	414.8

Table 10
Reliability index and reliability.

Iteration times	Reliability index	Reliability
1	2.392	0.99163
2	2.503	0.99393
3	2.472	0.99700
4	2.464	0.99740
5	2.477	0.99328
6	2.478	0.99331

Table 11
The comparison of results and calculation efficiency between the improved method and conventional method.

Methods	Reliability	Iteration times	Number of sample points
Conventional method	0.9934	9	63
Improved method	0.9933	6	42

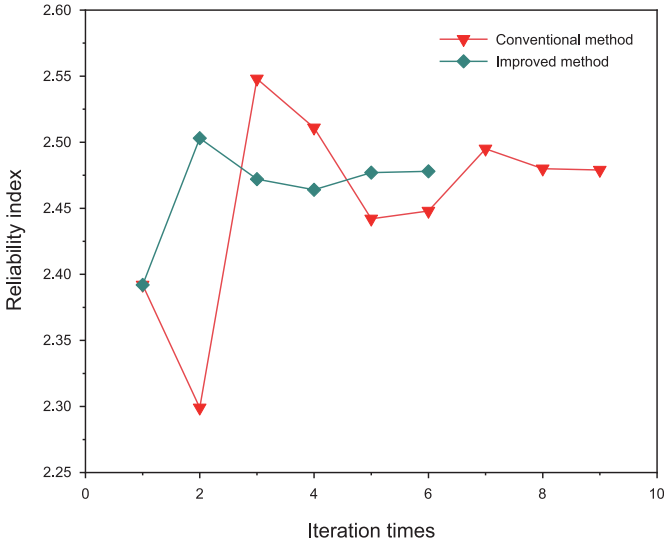

Fig. 12. The changing of reliability index with iteration times comparing two methods.

the proposed method in this paper can greatly improve the calculation efficiency.

CRediT authorship contribution statement

Yu Zhang: Writing – review & editing, Writing – original draft, Visualization, Validation, Supervision, Software, Resources, Project administration, Methodology, Investigation, Funding acquisition, Formal analysis, Data curation, Conceptualization. **Hong-Yu Zhang:** Writing – review & editing, Writing – original draft, Visualization, Validation, Supervision, Software, Resources, Project administration, Methodology, Investigation, Formal analysis, Data curation. **Ran Xia:** Supervision, Software, Resources, Methodology, Investigation, Formal analysis. **Si-Ao Jiang:** Software. **Fang Wang:** Resources, Project administration, Formal analysis, Data curation, Conceptualization.

Declaration of competing interest

The authors declare that they have no known competing financial interests or personal relationships that could have appeared to influence the work reported in this paper.

Acknowledgements

Financial support for this research was provided by the National Natural Science Foundation of China (Grant No. 52222111).

References

Akpan, U.O., Koko, T.S., Rushton, A., Tavassoli, M.E., 2007. Probabilistic fatigue reliability of large diameter steel catenary risers (SCR) for ultra-deep-water operations. In: ASME 2007 26th International Conference on Offshore Mechanics and Arctic Engineering, pp. 371–382. https://doi.org/10.1115/OMAE2007-29556.

Chen, K., Xia, F., Chen, J.L., Pan, C.Z., 2018. Introduction for subsea production system steel tube umbilical. Wire & Cable 1, 28–30. https://doi.org/10.16105/j.cnki.dxdl.2018.01.008.

Costello, G.A., 1997. Theory of Wire Rope. Mechanical Engineering Series, New York.

GB-50153, 2008. Unified Standard for Reliability Design of Engineering Structures. China.

Guo, H., 2016. Key Technologies of Umbilical Cable Design, Manufacture and Test for Underwater Production System. Petroleum Industry Press, Beijing.

Knapp, R.H., 1975. Nonlinear analysis of a helically armored cable with nonuniform mechanical properties in tension and torsion. In: Proceeding of IEEE/MTS Conference of Engineering in the Ocean Environment, pp. 155–164. https://doi.org/10.1109/OCEANS.1975.1155154.

Knapp, R.H., 1979. Derivation of a new stiffness matrix for helically armored cables considering tension and torsion. Int. J. Numer. Methods Eng. 14, 515–529. https://doi.org/10.1002/nme.1620140405.

Knapp, R.H., 1981. Torque and stress balanced design of helically armored cables. Journal of Engineering for Industry 103, 61–66. https://doi.org/10.1115/1.3184460.

Liu, J., An, Z.J., 2020. Fuzzy reliability analysis of contact fatigue strength of double shock sleeve movable teeth transmission based on an improved RSM. J. Mech. Strength 6, 1362–1368. https://doi.org/10.16579/j.issn.1001.9669.2020.06.014.

Liu, W.Q., Guo, H.Y., Chen, H.C., 2018. Analysis on the influence of armor layer parameters of umbilical cable on tensile behavior. Coast Eng. 39, 86–93. https://doi.org/10.3969/ji.ssn.1002-3682.2020.02.002.

Lu, Q.Z., 2013. Structural Design and Validation of Umbilical of Subsea Production System. Dalian University of Technology.

Nilsen, A.U., Hanson, T.D., 1995. Reliability based design of a 15" dynamic flexible gas export riser. In: The Fifth International Offshore and Polar Engineering Conference. International Society of Offshore and Polar Engineers, pp. 373–382.

Sævik, S., Gjøsteen, J.K.Ø., 2012. Strength analysis modelling of flexible umbilical members for marine structures. J. Appl. Math. 1–18. https://doi.org/10.1155/2012/985349.

Song, C.Y., Lee, J., Choung, J.M., 2011. Reliability-based design optimization of an FPSO riser support using moving least squares response surface meta-models. Ocean Eng. 38 (2–3), 304–318. https://doi.org/10.1016/j.oceaneng.2010.11.001.

Tang, M.G., Yan, J., Wang, Y., Yue, Q.J., 2014. Tensile stiffness analysis on ocean dynamic power umbilical. China Ocean Eng. 28, 259–270. https://doi.org/10.1007/s13344-014-0021-8.

Thies, P.R., Johanning, L., Smith, G.R., 2012. Assessing mechanical loading regimes and fatigue life of marine power cables in marine energy applications. Proc.

Inst. Mech. Eng. O J. Risk Reliab. 226, 18–32. https://doi.org/10.1177/1748006X11413533.
Wang, H.L., Zhang, Q.F., Quan, W.C., 2021. Study on dynamic performance of full-sea deep ROV non-metallic armored umbilical cable. High-tech Communications 31, 1293–1302. https://doi.org/10.1016/j.oceaneng.2021.109854.
Xia, J., Das, P.K., 2008. Probabilistic fatigue reliability analysis of deep-water steel catenary risers. In: ASME 2008 27th International Conference on Offshore Mechanics and Arctic Engineering, pp. 197–205. https://doi.org/10.1115/OMAE2008-57178.
Xia, R., Liu, H.L., Zhang, Z., Luo, D., Zhang, Y., 2021. Reliability analysis of umbilical based on fuzzy fault tree theory. Ocean Eng. 2, 153–161. https://doi.org/10.16483/j.issn.1005-9865.2021.02.016.
Xing, X.S., Yan, W., Deng, J.G., Zhang, C.Y., 2012. Influences of deepwater current velocity profile on transverse load on marine riser. Pet. Eng. Constr. 4, 8–10. https://doi.org/10.3969/j.issn.1001-2206.2012.04.003.
Xu, J.J., 2019. The Fatigue Optimization Design and Reliability Analysis of Umbilical in Subsea Production System. Dalian University of Technology.
Yan, J., Yang, Z.X., Zhao, P.P., Hu, H.T., Lu, Q.Z., Yue, Q., 2018. Reliability analysis of section strength of umbilical in ocean engineering. Chin. Sci.: Physics, Mechanics and Astronomy1 113–119. https://doi.org/10.1360/SSPMA2017-00157.
Yang, X.Y., Lv, H.N., Yang, J.M., Sun, P.F., 2023. Research on axial tension response characteristics of umbilical cable in deepsea mining truck deployment and recycling. Ocean Eng. 41, 128–138. https://doi.org/10.16483/j.issn.1005-9865.2023.05.012.
Yu, B.F., Su, F., 2008. New application of carbon composites in the offshore oil/gas industry. Mater. Eng. (Modena, Italy) 1, 182–185. https://doi.org/10.3969/j.issn.1001-4381.2008.z1.034.
Zhang, Y., Guo, Z.S., Zhao, H.K., Ma, G.Y., Zhang, F.F., 2021a. Analysis of torsional instability and reliability of marine flexible pipelines. Ocean Eng. 228, 108947. https://doi.org/10.1016/j.oceaneng.2021.108947.
Zhang, S.H., Wei, Y.G., Tian, H.J., Hu, X.Y., Cao, Y.G., 2019. Parameter sensitivity analysis of umbilical cable static strength considering friction. China Petroleum Machinery 47, 34–40. https://doi.org/10.160820/j.cnki.issn.1001-4578.2019.03.007.
Zhang, Z., Xia, R., Zheng, L.J., Ma, G.Y., Zhang, Y., 2021b. Reliability analysis of umbilical in full lifecycle based on phase mission system Bayesian network method. Ocean. Eng. 124–133. https://doi.org/10.16483/j.issn.1005-9865.2021.04.014.
Zhao, P.P., 2017. Reliability Analysis and Optimization Design of Umbilical Cable Structure in Subsea Production System. Dalian University of Technology.
Zhao, D., Lu, X.D., Pang, D.H., Leng, X.S., 2022. Study on environmental characteristics of the South China Sea current and its influence on deepwater drilling unit. China Resources Comprehensive Utilization 40, 65–67. https://doi.org/10.3969/j.issn.1008-9500.2022.02.019.
Zhu, Q.B., 2017. Mechanical Properties and Fatigue Analysis of Umbilical Cables. Harbin Engineering University.